Causes of Spurious Echoes by Ultrasonic Wave Simulation

by

H.A.J. Froeling

to obtain the degree of Bachelor of Science in Applied Physics
at the Delft University of Technology,
to be defended publicly on Monday May 12, 2017 at 09:30 AM.

Student number: 4258908
Project duration: February 13, 2017 – June 7, 2017
Thesis committee: S. Mastromarino, TU Delft (TNW)
Dr. ir. M. Rohde, TU Delft (TNW), supervisor
Prof. dr. ir. J.L. Kloosterman, TU Delft (TNW)

An electronic version of this thesis is available at http://repository.tudelft.nl/ and
http://www.nera.rst.tudelft.nl/en/publications/

TU Delft

Nomenclature

Roman characters

A	Amplitude	$[V]$
B	Bulk modulus	$[Pa]$
c	Wave velocity	$[m \cdot s^{-1}]$
d	Depth fluid	$[m]$
E	Young's modulus	$[Pa]$
f	frequency	$[Hz]$
k	Wavenumber	$[rad \cdot m^{-1}]$
p	Pressure	$[Pa]$
S	Surface	$[m^2]$
$\vec{u}$	Particle displacement vector	$[m]$
$\vec{v}$	Particle velocity vector	$[m \cdot s^{-1}]$
$\hat{v}$	Normal velocity of particle	$[m \cdot s^{-1}]$
V	Volume	$[m^3]$
Z	Impedance	$[Pa \cdot s \cdot m^{-1}]$

Greek characters

α	Angle of incidence	$[deg]$
α_F	Attenuation coefficient of fluid	$[dB \cdot m^{-1}]$
β	Angle of reflection	$[deg]$
γ	Angle of refraction	$[deg]$
$\partial\Omega$	Boundary	$[m^2]$
λ	Wavelength	$[m]$
λ_l	1^{st} Lamé parameter	$[Pa]$
μ_F	Viscosity of fluid	$[Pa \cdot s]$
μ_l	2^{nd} Lamé parameter	$[Pa]$
ρ	Density	$[kg \cdot m^{-3}]$
$\bar{\sigma}$	Stress tensor	$[Pa]$
χ	Compressibility	$[Pa^{-1}]$
ω	Angular frequency	$[rad \cdot s^{-1}]$
Φ	Dilation	$[m \cdot s^{-1}]$
Ψ	Rotation vector	$[m \cdot s^{-1}]$
Ω	Domain	$[m^3]$

Subscripts

c	Critical angle
F	Fluid properties
l	Lamé parameter
L	Longitudinal wave
S	Shear wave

Dimensionless numbers

CFL	Courant–Friedrichs–Lewy number
$\vec{n}$	Normal vector
R	Reflection coefficient
RR	Ratio of the radius of the transducer to the rod
$\bar{\epsilon}$	Strain tensor
T	Transmission coefficient

Abstract

An important issue for the assessment of the MSR's is the selection of the molten salt compositions, where many aspects should be taken in consideration. One section of the SAMOFAR project investigates the behavior of the molten salts. Due to the radioactivity and corrosiveness, only a small amount of the salt is usable and therefore traditional techniques cannot be used for the determination of the thermodynamic properties. Concerning these conditions a valid way to measure this properties is by using ultrasound.

Ultrasonic measuring relies on measuring the fraction of reflected waves, which are affected by the fluid. Since the temperature of the liquid is above 500°C it is not possible to use a transducer in contact with the liquid and a buffer rod has to be used to dissipate the heat. The disadvantage of using a buffer rod is that the reflected waves are not only affected by the properties of the fluid, but also by the properties of the rod. The combination of the additional signals and the desired signals are called spurious echoes.

In this research all reflection and transmission coefficient are derived in order to understand the behavior of the waves at the boundaries. Next, simulations affirm the existence of spurious echoes and assigned to different types of waves. Head waves are created by mode conversion of the emitted signal at the boundaries of the rod. Subsequently, longitudinal waves are created by mode conversion of head waves and have large contribution to the spurious echoes. At last, there is shown that the production of head waves can be reduced by changing the material properties.

Contents

1

Introduction

The present energy demand is gigantic and still increasing. Traditional energy sources, such as coal, does affect the global warming and sustainable energy sources are generally not efficient enough. Therefore, nuclear energy can be a key player in the current energy problem. Unfortunately, the nuclear energy became unpopular after the historic nuclear disasters in Three Mile Island (1979) and Chernobyl (1986). Moreover, the traditional energy sources are still cheaper to use. To compete with these sorts of energy, a constant improvement of nuclear energy is needed in order to support the future role of nuclear power plants and confront the public debate about nuclear energy. In 2000 several countries joined together to propose, seven new type of Generation IV nuclear energy systems were proposed. Safety, sustainability, reliability, economic competitiveness and proliferation resistance are the main goals of the Generation IV Nuclear Reactors [1], which are expected to start entering commercial operation from 2030.[2]

1.1. Molten Salt Fast Reactor

The Molten Salt Fast Reactor (MSFR) is one type of the Molten Salt Reactors that are part of the six Generation IV reactors. This reactor was actually already invented by the end of the 50s, by Oak Ridge National Laboratory. Despite all positive research revealing, there was decided to cancel further development in order to attempt another revival of the Liquid-Metal-cooled Fast Breeder Reactor program, which was compatible with the Uranium/Plutonium-cycle. This choice was made by the fact that the MSFR was not only a new reactor, but also a whole new fuel cycle [3]. In the beginning of this century the concept of the Molten Salt Fast Reactor was rediscovered and proposed to be one of the Generation IV reactors. In essence, a MSFR is a vessel that contains a hot liquid salt in which a nuclear reaction takes place. The peculiarity and innovation of this nuclear reactor is the use of this liquid fuel, which serves both as nuclear fuel as a heat transfer medium resulting in several advantages [1, 3], especially for the reactor safety.

One risk of nuclear reactors is the meltdown of the reactor's solid core, whereby radioactive materials are able to breach all containment and escape into the environment, resulting in radioactive contamination and potentially leading to radiation poisoning of population. For the Molten Salt Fast Reactor the nuclear fuel is the molten salt itself, which is molten already and therefore a nuclear meltdown is excluded. In addition, the reactor operates only at atmospheric pressure, so the risk o fan explosion is excluded. The liquid property of the salt allows a draining system to dump the core into passively cooled critically-safe tanks to respond to emergencies, which includes freeze-plugs that would melt as soon as electric power is lost or the salt seriously overheats. This confirms once again that the MSFR is an extremely safe reactor.

Next to all safety advantages, the MSFR has great advantages in the field of efficiency and sustainability. The reactor can run at higher temperatures than water-cooled reactors for a higher thermodynamic efficiency, while staying at low vapor pressure. The excellent heat transfer capacity of the molten salts allows a quickly transfer of energy out of relatively small reactor core. In addition, the continuous fuel recirculation in the reactor provide also low radioactivity inventory. The produced waste reaches natural levels of radiotoxicity

after just a couple of centuries, which is low compared to the current nuclear waste which has a radiotoxicity of hundreds of years.

However, yet the MSFR concept is still in development phase. The investment costs are enourmous and there is no licensing framework where it can be built on, because all research data of Oak Ridge National Laboratory is in the meantime outdated. In the Safety Assessment of the Molten Salt Fast Reactor (SAMOFAR) project, eleven European universities and research institutes cooperate to demonstrate the safety of the MSFR, to deliver a breakthrough in nuclear safety and optimal waste management.

1.2. Ultrasonic Wave Measuring

An important issue for the assessment of the MSR's is the selection of the molten salt compositions, where many aspects should be taken in consideration. One section of the SAMOFAR project investigates of the behavior of the molten salts. Therefore, it is essential to know the thermodynamic properties these liquid in order to predict the behavior in all circumstances. The thermal conductivity, heat capacity, density and viscosity are essential characteristics to understand the behavior of the salt. While facilities for the measurement of heat capacity and thermal conductivity exist, there are not yet accurate techniques for measuring the density and viscosity of the salts. Traditional techniques cannot be used because of the small amount of salt usable due to its radioactivity and corrosiveness. Concerning these conditions a valid way to measure this properties is by using ultrasonic sound waves. Additional advantages of using ultrasound for measuring the fluid properties is that it is possible to measure the density and viscosity with the same device.[1]

A transducer consisting of a piezoelectric element generates ultrasonic waves which are transmitted through the fluid. Due to the viscous properties of the fluid the waves are attenuated. This technique relies on measuring the fraction of reflected waves, which are affected by the fluid. Since the salt is melted above 500°C, the temperature range for the viscosity measurement is 500°C and 1000°C. At this temperature it is not possible to use a transducer in contact with the liquid and a buffer rod has to be used to dissipate the heat. The disadvantage of using a buffer rod technique is that the reflected waves are not only affected by the properties of the fluid, but also by the properties of the rod. Several physical phenomena create additional signals in the reflected data and often interfere with the desired signals. **The combination of the additional signals and the desired signals are called trailing- or spurious echoes.** Some studies say that tapering or cladding of the rod lead to a reducing of these spurious echoes [4, 5]. This is desirable because, the spurious echoes reduce the measurement's accuracy.

1.2.1. Aim of this Research

In this research will seek for the causes of these spurious echoes. Several studies have shown that the origin of the spurious echoes could be the cause of interaction of the waves with the boundaries [6, 7]. In order to verify those causes, ultrasonic waves will be simulated with the simulation software COMSOL Multiphysics. Hereby, it is important that the simulations represent the physical behavior of the waves accurately and in order to prevent poorly configured models, there will be looked carefully for the size of the mesh elements. The above results in the following specific research questions:

- What are the useful physical explanations for the wave behavior in the rod and at the boundaries?
- What are essential numerical considerations for accurate simulations?
- What are the causes of spurious echoes on the basis of the simulation outcomes?

I

Physics of Ultrasound

2

Theory of Acoustics

Humans can hear sound waves with frequencies between about 20 Hz and 20 kHz. Sound above 20 kHz are called ultrasound and below 20 Hz infrasound. Sound is the audible vibration of particles that propagates as a mechanical wave of pressure through a transmission medium [1].

Historically, there is a distinction between transmission media based on their qualitative differences in properties and divided into three different states of matter: solid, liquid and gas. In solids, the particles are closely packed together and the forces between particles are strong, so that the particles cannot move freely but can only vibrate. For a liquid the molecules have enough energy to move relative to each other and the structure is mobile, but the inter-molecular forces are still important. Gas acts as a fluid where the molecules have very weak and the molecules can move freely and fast. Although, fluids and gases have different properties, they have in common that they both have weak particle bonding and therefore have no rigidity, a lack of the ability to resist deformation. This is essential for the waves inside the transmission medium, because the behavior of waves is mainly based on the properties of the medium where the wave is propagating in.

Acoustic ultrasonic waves are made by disturbing a medium with a source, resulting in a local pressure difference. This change of pressure is associated with a flow of energy propagating through the medium. This flow of energy can be described by an mechanical wave where, the wave crests are the pressure maxima, while the troughs represent the pressure minima [8]. Partial differential equations describe these motions of these waves. The differential wave equation for solids is different than the equation for fluids and gases, due to the presence of rigidity owing to the strong particle bonding. The reasons for setting up these differential wave equation will be clear in the subsequent sections, where the behavior of the waves at the boundaries will be treated.

There are different types of waves. The waves in fluids are called compression, pressure or longitudinal waves. Since fluids do not have the ability to resist deformation the waves only propagate under the direct action of the force and are always directed in the motion of the particles. Another type of wave is the shear wave of transverse wave. For shear waves the particles move perpendicularly to their direction of propagation and need therefore a medium rigid enough to propagate. They can only propagate through solids, since these have strong particle bonding. Liquids do not have the same shear strength, hence, shear waves do not propagate through liquids [9**?** , 10]. **Waves propagating in the direction parallel to the motion of the particles are termed longitudinal waves and the waves directed perpendicular to the movement of particles are called shear waves.**

For the elaborations of the wave equations, some important mathematical operations are used. Firstly, $\frac{d}{dt}$ and $\frac{\partial}{\partial t}$ are the time derivative and the partial derivative to time, respectively. ∇ is the gradient, that is the partial derivative with respect to the coordinates of the associated coordinate system. Together they are the most important mathematical operations.

2.1. Bulk Waves in Fluids

Characteristic of liquids is that they all have a specific viscosity. The viscosity of fluids is the measure of its resistance to flows and can be denoted as the ratio of the shearing stress to the velocity gradient. Fluids can be divided in two main groups: inviscid and viscous fluids, where for inviscid fluids the viscosity approaches zero. The wave equation for inviscid fluids will be derived first. The fundamental equations are based on Reynold Transport Theorem, resulting in three equations for the convervation of mass, momentum and energy. The derivation of these conservation equation are found in Appendix A. In this section we will use the final form of each.

2.1.1. Acoustic Wave Equation

We assume that the wave motions in the models are small perturbations. Hence, the velocity, density and deformation have only comparatively small changes, that is, small oscillations around the equilibrium state characterized by the steady-state value and the change in geometry can be neglected. For fluids, the relation of pressure to the change in velocity is defined in Newton's second law of motion, found by solving the equation of momentum. Newton's law can be expressed as [11]

$$\vec{\nabla} p = -\rho \frac{\partial \vec{v}}{\partial t}. \tag{2.1}$$

For small variations in pressure the relation of the applied pressure to the compression of the fluid can by expressed in Hooke's law, the equation of deformation. The deformation of a fluid can be expressed by the compressibility or its inverse, the bulk modulus. Here, the minus sign denotes that the pressure is inversely proportional to the change in displacement [11]

$$\frac{\partial p}{\partial t} = -\frac{1}{\chi} \nabla \cdot \vec{v}. \tag{2.2}$$

Combining the equation of deformation (2.2) and equation of motion (2.1), we can obtain a wave equation for the pressure field [1]. We multiply the the equation of deformation (2.2) for $\rho\chi\frac{\partial}{\partial t}$ and taking the gradient of the equation of motion (2.1)

$$\frac{\partial}{\partial t}\left(\frac{1}{\rho c_F^2}\frac{\partial p}{\partial t}\right) = \frac{\partial}{\partial t}(-\nabla \cdot \vec{v}), \tag{2.3}$$

$$\vec{\nabla} \cdot (\vec{\nabla} p) = \vec{\nabla} \cdot \left(-\rho \frac{\partial \vec{v}}{\partial t}\right). \tag{2.4}$$

Combining expressions (2.3) and (2.4) we obtain the acoustic wave equation for an inviscid fluid

$$\frac{1}{c_F^2}\frac{\partial^2 p}{\partial t^2} - \nabla^2 p = 0. \tag{2.5}$$

In the case of a viscous fluid, the pressure force is not the only force acting on the fluid but there will be shear force. The relation is described by the Navier-Stokes equation, where will be assumed that the fluid is a Newtonian fluid and therefore the viscous stresses arising from its flow are lineary. For the scope of this research we will not solve the Navier-Stokes equation in this report. A clear derivation of the solution of the Navier-Stokes equation can be found in [1]. The solution of the Navier-Stokes equation will give a additional factor, proportional to the viscosity and the acceleration of the particles. The new equation of motion can now be defined as

$$\vec{\nabla} p + \rho \frac{\partial \vec{v}}{\partial t} = \frac{4\mu_F}{3}\frac{\partial^2 \vec{v}}{\partial t^2}. \tag{2.6}$$

Combining this new equation of motion (2.6) and the equation of deformation (2.2) is resulting in

$$\nabla^2 p = \frac{1}{c_F^2}\left(\frac{\partial^2 p}{\partial t^2} + \frac{4\mu_F}{3}\frac{\partial \nabla^2 p}{\partial t}\right). \tag{2.7}$$

The last equation is the final form of the acoustic wave equation for viscous fluids. **As a conclusion, it can be confirmed that longitudinal pressure waves travel with a speed of $c_F = \sqrt{\frac{B}{\rho}}$ through fluids where ρ is the density and B the bulk modulus, for isentropic fluids.**

2.2. Bulk Waves in Solids

In general, liquids are compressible compared to solids. This is why the acoustic pressure and the compressibility are commonly used as parameters for liquid. In solids, the displacement, stress and elastic constants are more appropriate parameters [12]. In this chapter we will see how the mutually perpendicular longitudinal and transverse waves which are able to propagate in solids can be defined in one displacement vector $\vec{u} = u_L + u_S$.

The derivation of the differential wave equation in solids shows similarities with the derivation of the wave equation for fluids. Such as for the wave equation for fluids we assume that the solid medium is isotropic, so the properties are the same regardless of different orientations. Newton's law and Hooke's law can be used for the derivation of the elastic wave equation. A brief explanation of concepts such as deformation, strain tensor, stress tensor and the moduli of elasticity will be presented. The derivation of all these parameters is complex and out of scope of this research.

2.2.1. Elasticity

Solids are elastic materials due to the strong particle bonding. They respond to an applied force by deforming and return to the original shape upon the removal of the applied force. Rigidity is the property of a solid body to resist deformation [12]. For elastic materials, the relative deformation of the solid is called strain and the forces that occur in the solid are described as stresses. This produces small oscillation of particles in the solid, which are called vibrations. If the strains are sufficiently small, they are related to the displacement by the linearized strain tensor ϵ, which is defined by [11, 13]

$$\bar{\epsilon} = \frac{1}{2}\left((\vec{\nabla}\vec{u}) + (\vec{\nabla}\vec{u})^c\right), \tag{2.8}$$

where $\vec{u}$ is the displacement vector of the particles and states that there are two different strains possible in solids: tensile strain and shear strain. These are mutually perpendicular and can be seen in figure 2.7.

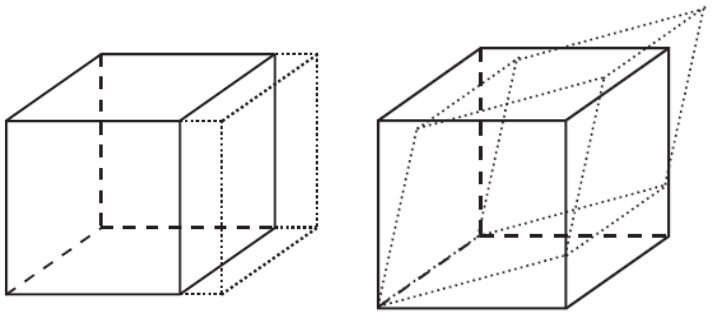

(a) Tensile strain (b) Shear strain

Figure 2.1: Tensile and shear strain for a unit cube [12]

Neglecting body forces such as gravity, solely the forces acting on the faces of the cube will lead to deformation

of the cube, which can be described by the strain tensor, treated previously. The components of the applied forces, seen in figure 2.2 can be classified into two major classes: normal component, which will give rise to the compressive or tensile stresses and tangential component, giving rise to shear stresses [12].

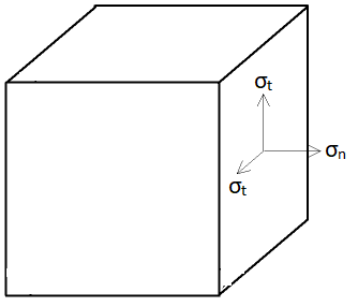

Figure 2.2: Forces acting on unit cube: normal component (σ_n) and tangential component (σ_t)

Fluids experience only shear strain for a shear stress, where solids are able to experience strain for both tensile and shear stress. The interaction between the strain and stress in solids can be defined by Hooke's law[11, 13]

$$\bar{\sigma} = \lambda(\nabla \cdot \vec{u})\bar{I} + 2\mu\bar{\epsilon}(\vec{u}). \tag{2.9}$$

Hooke's law applies for small displacements, with $\vec{\sigma}$ is the stress and λ and μ are Lamé constants, defining the elastic properties. These Lamé constants are the constants historically chosen to describe the elastic properties of an isotropic solid. There are four parameters related to the Lamé constants, which have found practical use as they are directly related to measurements [12]:

- Young's modulus E is defined as the ratio of tensile stress to the tensile strain,
- Poisson's ratio ν is given by the ratio of shear strain to the tensile strain,
- Bulk modulus B is the elasticity corresponding to compression ,
- The Lamé parameter μ is equivalent to the shear modulus and is defined as the ratio of shear stress to the shear strain.

2.2.2. Elastic Wave Equation

Newton's second law of motion in solids can be expressed as

$$\vec{\nabla} \cdot \bar{\sigma} = \frac{\partial^2 \vec{u}}{\partial t^2}, \tag{2.10}$$

which relates the stress $\vec{\sigma}$ to the particle displacement $\vec{u}$. Combining Newtons law (2.10) with Hooke's law (2.9), we obtain the vector-valued **Navier-Cauchy equation** for the media [13]

$$(\lambda + \mu)\vec{\nabla}(\vec{\nabla} \cdot \vec{u}) + \mu\lambda^2\vec{u} = \rho\frac{\partial^2 \vec{u}}{\partial t^2}, \tag{2.11}$$

with $\vec{u} = \vec{u_L} + \vec{u_S}$. This equation comprises the whole mechanical equilibrium of an elastic solid. For convenience we define the dilation of a material by $\vec{\nabla} \cdot \vec{u} = \Delta$ and the rotation vector $\vec{\omega}$ by $\vec{\omega} = \frac{1}{2}\vec{\nabla} \times \vec{u}$, so we may express Navier-Cauchy equation as

$$(\lambda + 2\mu)\vec{\nabla}\Delta - 2\mu\vec{\nabla} \times \omega = \rho\frac{\partial^2 \vec{u}}{\partial t^2}, \tag{2.12}$$

that contributes to the clarity of the derivation of the longitudinal and especially the transverse wave equation, in the end. For the longitudinal waves the particles of the medium move in the direction of propagation and so has no curl, $\nabla \times \vec{u_L} = 0$. The displacement vector for the shear waves has no divergence, $\nabla \cdot \vec{u_S} = 0$. So for the longitudinal wave we perform the operation of divergence on the Navier-Cauchy equation, which yields

$$(\lambda + \mu)\vec{\nabla} \cdot \vec{\nabla}(\vec{\nabla} \cdot \vec{u}) + \mu\vec{\nabla} \cdot \lambda^2 \vec{u} + \rho f = \rho\vec{\nabla} \cdot \frac{\partial^2 \vec{u}}{\partial t^2}, \tag{2.13}$$

with $\nabla^2 = \vec{\nabla} \cdot \vec{\nabla}$, $\vec{\nabla} \cdot (\nabla^2 \cdot \vec{u}) = \nabla^2(\vec{\nabla} \cdot \vec{u})$ and $\vec{\nabla} \cdot \vec{u} = \Delta$, the dilation reduces to

$$\nabla^2 \Delta = \frac{\rho}{(\lambda + 2\mu)} \frac{\partial^2 \Delta}{\partial t^2}. \tag{2.14}$$

We thus can conclude that the speed of sound for longitudinal waves, i.e. a change in volume, is

$$c_L = \sqrt{\frac{\lambda + 2\mu}{\rho}}. \tag{2.15}$$

If the vector operation of curl is performed for the transverse waves, we obtain

$$(\lambda + 2\mu)\vec{\nabla} \times \vec{\nabla}\Delta - 2\mu\vec{\nabla} \times (\vec{\nabla} \times \omega) = \rho\vec{\nabla} \times \frac{\partial^2 \vec{u}}{\partial t^2}. \tag{2.16}$$

Recalling $\vec{\omega} = \frac{1}{2}\vec{\nabla} \times \vec{u}$ and $\vec{\nabla} \cdot (\vec{\nabla} \times \vec{u}) = 0$ we get

$$\nabla^2 \vec{\omega} = \frac{\rho}{\mu} \frac{\partial^2 \vec{\omega}}{\partial t^2}. \tag{2.17}$$

This is the elastic wave equation for transverse waves in an elastic medium, with wave speed $c_S = \sqrt{\frac{\mu}{\rho}}$. **Summarizing, two waves can propagate in an unbounded elastic medium. Longitudinal waves with a velocity of $c_L = \sqrt{\frac{\lambda+2\mu}{\rho}}$ and shear waves with a velocity of $c_S = \sqrt{\frac{\mu}{\rho}}$.**[13]

2.3. Plane Wave Solution and Acoustic Impedance

—— The previous derived wave equations show many similarities. Both equation In this section we are going to look at the solution of the acoustic wave equation, but since the wave equation shows a lot of similarities with the elastic wave equation, the solutions are also valid for solids. ——

One-dimensional wave equation can be solved exactly via separation of variables, where the displacement of the particles $u(x,t)$ can be split up into space-dependent and time-dependent part resulting in $p(x,t) = X(x)T(t)$. The solution, the so called plane wave equation, has the general form

$$p(x,t) = p_0 e^{\pm i(kx - \omega t)}, \tag{2.18}$$

where ω is the angular frequency, k is the wave number, that is equal to $\frac{\omega}{c}$ in case of a wave propagating in a inviscid fluid, $\pm$ determines the direction the wave travels, where the minus sign represents propagation in the 'positive' direction [14]. The particle velocity must also be considered, because this tells us how fast the molecules in the medium are moving. Acoustic impedance is the ratio of acoustic pressure to flow and allows us the simplify the complex behavior of the waves at the boundaries. We are going to use the plane wave

solution of a pressure wave in fluids to derive the expression for the acoustic impedance, which derivation is also valid for solids. In order to simplify the solutions the Fourier transforms are used, using $\mathscr{F}[\frac{d}{dt}x(t)] = i\omega X(i\omega)$:

$$\hat{p}(x,\omega) = F(\omega)exp^{-ikx}, \tag{2.19}$$

$$-\frac{\partial \hat{p}(x,\omega)}{\partial x} = i\omega\rho\hat{v}(x,\omega), \tag{2.20}$$

and combining them, the particle velocity is

$$\hat{v}(x,\omega) = \frac{1}{\rho c}F(\omega)exp^{-ikx}. \tag{2.21}$$

Determine the acoustic impedance, the ratio between the pressure and the particle velocity, for plane waves yield

$$Z \equiv \frac{\hat{p}}{\hat{v}} = \frac{F(\omega)exp^{-ikx}}{\hat{v}(x,\omega) = \frac{1}{\rho c}F(\omega)exp^{-ikx}} = \rho c. \tag{2.22}$$

So the acoustic impedance relates the characteristics of a sound wave to the properties of the medium in which it is propagating. [14] This is the reason why the previous determined velocities are so important and the reason for the measuring the density in the experiments. Note that the impedance for solids and fluids are not equal, due to difference in density and the velocity of the sound determined by the differential wave equations. Lastly, the unit of acoustic impedance is *Rayl*, what equals *Pa s/m*.

The speed of wave for fluids is $\sqrt{\frac{B}{\rho}}$. In solids, the longitudinal sound waves have a velocity of $\sqrt{\frac{\lambda+2\mu}{\rho}}$, in terms of the bulk modulus being $\sqrt{\frac{B+4\mu/3}{\rho}}$. **Longitudinal waves propagate faster in solids than fluids.**

2.4. Wave Characteristics at the Boundaries

Till now we have looked at the bulk waves propagating in the bulk of the medium only. We derived the solutions of the differential wave equations describing the propagation of waves, characterized by the material properties. In this section where shall investigate some aspects of waves impinge on boundaries, which even in the simplest case are rather complicated. We will apply specific boundary conditions to the wave solutions which determine the local behavior of the waves near the boundaries. These conditions rely on the continuity of certain quantities, like displacement or stress. In general the behavior of the sound waves are much in the same way as the behavior of optical light passing through a boundary between two different isotropic media. A specific fraction of the energy of the incoming wave will reflect at the interface, while the remaining energy will transmit into the next medium. Due to different material properties the transmitted wave will refract with a specific angle. **The relationship between the angles are given by Snell's law, where the angles are with respect with the *normal*:**

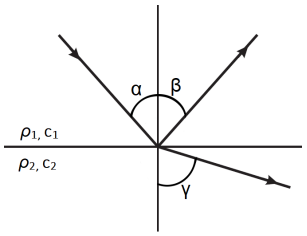

Figure 2.3: Definitions of angles

$$\frac{sin(\alpha)}{c_1} = \frac{sin(\gamma)}{c_2}. \tag{2.23}$$

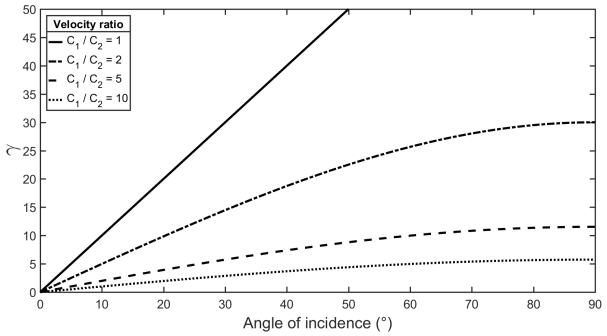

Figure 2.4: Snell's law: angle of refraction (or reflection) for incoming angles by and the influence of the velocity ratio

The angles are defined in figure 2.3, that will be used for the rest of this report. Figure 2.4 shows the influence of the wave velocity for the refraction angle. For equal wave velocities the angle of reflection angle will be the same as the angle of incidence. Note that therefore $\beta = \alpha$, in figure 2.3.

In this section we are going to look at three different interfaces. The first interface is a relative simple case and useful to get a general idea of the behavior of sound waves at the boundaries. The last to interfaces represent two situations in our setup.

- Fluid-Fluid Interface
- Solid-Air Interface
- Solid-Fluid Interface

2.4.1. Liquid-Liquid Interface

Even though we do not have the liquid-liquid interface in the experimental setup, it is a useful case where we can get a proper idea of the reflections and transmission of the waves at the boundary. Furthermore, the great benefit of Snell's law and the convenience of the acoustic impedance will be established. Consider a plane wave travelling in the (x,y)-plane from liquid 1 (ρ_1, c_1) to liquid 2 (ρ_2, c_2). Since the two media must stay in intimate contact at a perfect interface the boundary conditions are [15]:

1. Continuity of pressure: $p_1 + p_1' = p_2$,

2. Continuity of normal velocities: $\hat{v_1} + \hat{v_1}' = \hat{v_2}$,

where p_1' and $\hat{v_1}'$ are the pressure and the normal velocity of the reflected wave, respectively. The continuity of pressure can only be fullfilled if Snell's law is applied. Solving the continuity of the normal velocity by using Snell's law gives the following coefficients: [12]

$$R = \frac{Z_2 \cos\alpha - Z_1 \cos\gamma}{Z_2 \cos\alpha + Z_1 \cos\gamma}, \tag{2.24}$$

$$T = \frac{2Z_2 \cos\alpha}{Z_2 \cos\alpha + Z_1 \cos\gamma}, \tag{2.25}$$

where Z is the acoustic impedance (ρc) by (2.22). **R and T are the reflection and transmission coefficient, respectively. These denotes the ratio of the reflected or transmitted amplitude and the amplitude of the incoming wave.** In figure 2.5 these coefficient are given as a function of the incident angle α, based on equations (2.23), (2.24) and (2.25).

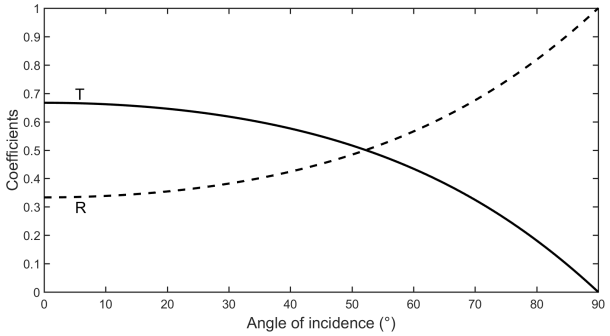

Figure 2.5: Reflection and refraction amplitude coefficients for incoming angles, with equal density and $\frac{c_1}{c_2} = 10$.

So for $Z_1 > Z_2$ the transmission coefficient decreases and the reflection coefficient increases for increasing α. These coefficients describe how large the amplitude of the reflected or transmitted waves are after interaction with the boundary. For further investigation of the influence of the material properties to the coefficients the transmission coefficient will be plotted in figure 2.6 against the angle of incidence with $c_1/c_2 = 2$ and a logaritmic decreasing ρ_1/ρ_2, i.e. 1, 1/10, 1/100 and 1/1000.

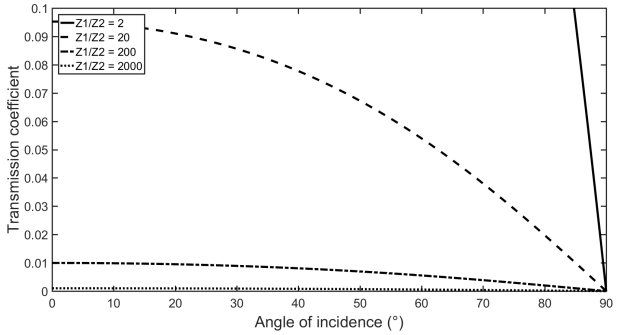

Figure 2.6: Transmission coefficient for incident angles and different impedances, with $Z_1 > Z_2$.
Increasing impedance difference results in a reduction of the transmission coefficient

The reflection and transmission coefficients can also be expressed in terms of energy (intensity), instead of displacement amplitudes. The energy of the waves is equal to the squared wave amplitude multiplied by the impedance depending upon the medium in which the wave is propagating [16]. Reflection and transmission coefficient (2.24) and (2.25) in terms of energy can be written as, where $R + T = 1$, for the conservation of energy:

$$R = \frac{Z_1}{Z_1}\left(\frac{Z_2\cos\alpha - Z_1\cos\gamma}{Z_2\cos\alpha + Z_1\cos\gamma}\right)^2 = \left(\frac{Z_2\cos\alpha - Z_1\cos\gamma}{Z_2\cos\alpha + Z_1\cos\gamma}\right)^2, \tag{2.26}$$

$$T = \frac{Z_2}{Z_1}\left(\frac{2Z_2\cos\alpha}{Z_2\cos\alpha + Z_1\cos\gamma}\right)^2 = \frac{4Z_1Z_2\cos^2\alpha}{(Z_2\cos\alpha + Z_1\cos\gamma)^2}. \tag{2.27}$$

2.4.2. Solid-Air Interface

This interface is present at the edge of the rod, where the solid is surrounded with air. In the previous section we saw that for enormous impedance differences, the transmission coefficient can be neglected. Since the impedance of solids is generally larger than the impedance of air, we can consider the solid-air interface as a *free boundary*, where the air will be considered as vacuum. Therefore the impedance difference is approaching infinity and no transmission will occur. In solids, the incoming wave can be a longitudinal or a transverse wave with each its own behavior at the free boundary interface, see figure 2.7a and 2.7b.

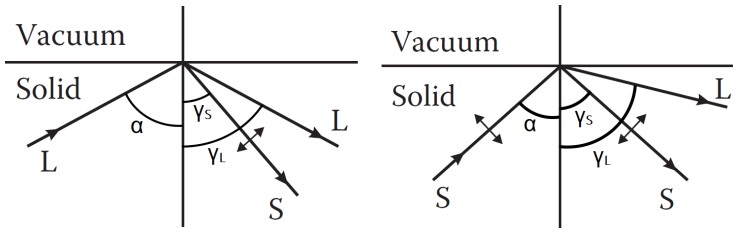

(a) Incoming longitudinal wave (b) Incoming shear wave

Figure 2.7: Reflection angles for incoming longitudinal and shear wave at a free boundary

Due to the fact that there are two waves able to propagate, conversion between the modes of these waves can occur. This is based on the fact that one form of wave energy can be transformed into another form [17]. For example, when a longitudinal waves hits an interface at an angle, some of the energy can cause particle movement in the transverse direction to start a shear wave. This mode conversion occurs when a wave encounters an interface between materials of different acoustic impedances and the incident angle is not normal to the interface. Although, for both modes of incoming waves the boundary conditions are the same:

1. Zero normal stress
2. Zero tangential stress

Using Hooke's law for isotropic solids to derive the normal and tangential stresses and apply these to the boundary condition gives the following expressions regarding to the intensities [12, 18, 19]

$$R_{LL} = -\frac{\cos^2 2\beta - (c_S/c_L)^2 \sin 2\alpha \sin 2\beta}{\cos^2 2\beta - (c_S/c_L)^2 \sin 2\beta \sin 2\alpha}, \tag{2.28}$$

$$R_{LS} = \frac{2(c_S/c_L) \sin 2\alpha \cos 2\beta}{\cos^2 2\beta - (c_S/c_L)^2 \sin 2\beta \sin 2\alpha}, \tag{2.29}$$

$$R_{SL} = \frac{(c_S/c_L) \sin 2\alpha \cos 2\alpha}{\cos^2 2\beta - (c_S/c_L)^2 \sin 2\beta \sin 2\alpha}, \tag{2.30}$$

$$R_{SS} = \frac{\cos^2 2\alpha - (c_S/c_L)^2 \sin 2\alpha \sin 2\beta}{\cos^2 2\beta - (c_S/c_L)^2 \sin 2\beta \sin 2\alpha}, \tag{2.31}$$

where R_{LL} and R_{LS} are the coefficient for an incident longitudinal wave. R_{SL} and R_{SS} are for an incident shear wave. Furthermore, the following relations can be obtained from the previous equation [12]:

$$R_{LL} = -R_{SS}, \tag{2.32}$$

$$R_{LL}^2 + R_{LS} R_{SL} = 1. \tag{2.33}$$

Equations (2.28) - (2.31) are plotted in figure 2.8 and 2.9 where the material properties of copper are used, $\rho = 8930[^{kg}/_{m^3}]$, $c_L = 4760[^{m}/_{s}]$ and $c_S = 2325[^{m}/_{s}]$. At normal incidence ($\alpha = 0°$) all reflected angles are the same wave mode as the incident wave, for both cases. For increasing α one can see that a fraction of the incoming waves are converted into another wave mode. Due to the different speed of waves for every wave mode the angle of reflection is different as well, on the basis on Snell's law.

For the case of an incident shear wave, it may be seen that the velocity of the reflected wave is greater than the velocity of the incoming wave, which is inevitably due to $c_L > c_S$. There exists a critical value of the incidence angle for which the reflected longitudinal wave completely disappears. The critical angle for copper is defined by

$$\alpha_c = sin^{-1}\frac{c_S}{c_L} = 29.2°. \tag{2.34}$$

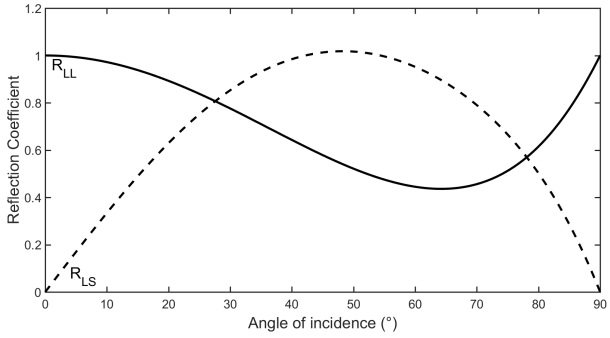

Figure 2.8: Reflection coefficient of longitudinal waves (R_{LL} and shear waves R_{LS} for incident angles of longitudinal wave at a free boundary

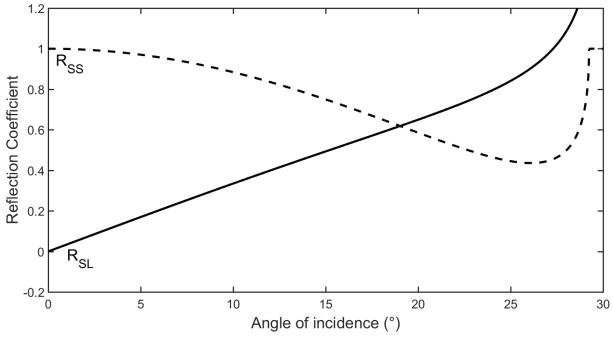

Figure 2.9: Reflection coefficient of shear waves (R_{SS} and longitudinal waves R_{SL} for incident angles of a shear wave at a free boundary, with critical angle of 29.2° for copper

2.4.3. Liquid-Solid Interface

The liquid-solid interface takes place at the end of the rod, we they waves in the solid transmitted into the fluid. Since we are going to solve the reflection and transmission coefficient in terms of energy the coefficients have many similarities with the coefficient for the solid-fluid interface. For both cases, the normal component of displacements and forces are balanced, so the boundary conditions for this interface are [12]:

1. Continuity of normal velocities
2. Continuity of normal stress
3. Zero tangential stress

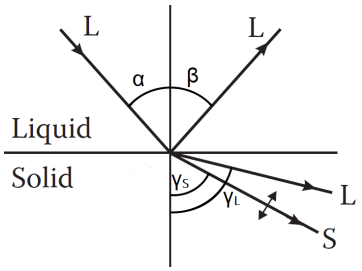

Figure 2.10: Angles of different waves for incident longitudinal wave at the liquid-solid interface

Solving these boundary conditions for the waves gives the reflection and transmission coefficients, again regarding to the energy of the waves [12, 20]:

$$R = \left(\frac{K - 2Z_F}{K}\right)^2, \tag{2.35}$$

$$T_L = \frac{4Z_F Z_L}{K^2}\cos^2 2\gamma_S, \tag{2.36}$$

$$T_S = \frac{4Z_F Z_S}{K^2}\sin^2 2\gamma_S. \tag{2.37}$$

The following substitution are used:

$$K = Z_L \cos^2 2\gamma_S + Z_S \sin^2 2\gamma_S + Z_F, \tag{2.38}$$

$$Z_F = \frac{\rho_F c_F}{\cos\alpha},\ Z_L = \frac{\rho c_L}{\cos\gamma_L},\ Z_S = \frac{\rho c_S}{\cos\gamma_S}. \tag{2.39}$$

and with $R + T_L + T_S = 1$. In order to discuss the formulae, we consider again copper as solid and glycerol as fluid ($c_F = 1920[^m/_s]$, $\rho_F = 1264[^{kg}/_{m^3}]$). The reflection and transmission coefficients are shown in figure2.11, with two different critical angles. The first critical angle of incidence (α_1), the angle of refraction of the pressure wave in the solid reaches 90° and thus, at this point the pressure wave disappears from the solid. This angle is given by $\alpha_1 = \sin^{-1}(\frac{c_f}{c_l})$. For the copper-glycerol interface is the first critical angle at 23.8°. In the solid for $\alpha > \alpha_1$ the incident P wave is completely transformed into the mode converted shear wave. The intensity of the latter rapidly increases at the expense of the reflected pressure wave. If we further increase the angle of incidence, the angle of refraction of the S wave also reaches 90° and at this point the S wave disappears as well. This second critical angle of incidence (α_2) is given by $\alpha_2 = \sin^{-1}(\frac{c_f}{c_s})$ and is for our interface 55.7°. For $\alpha > \alpha_2$ the reflection coefficient for the incident pressure wave in the liquid is equal to one since all other wave modes are no longer present.

2.5. Conclusion

From continuity requirements it follows that we are able to use Snell's law to determine the relationship of the angles. It enables us to set up coefficients of the reflected or transmitted wave as a ratio of the incoming wave as well. These coefficients can be expressed in terms of amplitude of energy. The amplitude expression differ for each material, where the energy expression does not. The coefficients in terms of energy describes the behavior of the waves at the boundaries the clearest and therefore we prefer this expression.

All interfaces encounter complex wave behavior. The solid-air interface can be considered as a free boundary, neglecting the transmission of waves into the air. Although, one form of wave energy can be transformed into another form, called mode conversion. The behavior of the waves at this boundary depends on the angle and mode of the incoming waves. For copper is this behavior stated in figure 2.8 and figure 2.9.

Since $C_F < C_L$ the fluid-solid interface has two critical angles, which for copper and glycerol are 23.8° and 55.7°. Later on, there will looked of waves with normal incidence, resulting in an enormous simplification of equations (2.35) and (2.36).

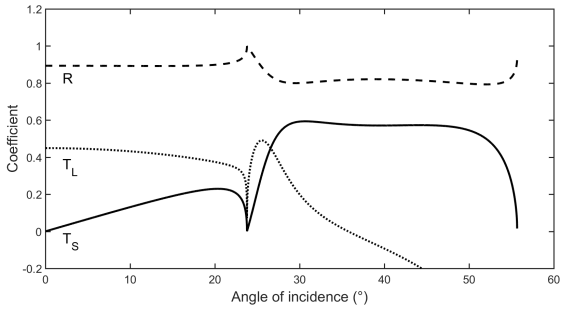

Figure 2.11: Reflection coefficient (R) and transmission coefficients of longitudinal waves (T_L) and shear waves (T_S) in solid for the fluid-solid interface

3

Experimental Background

Ultrasound waves are generated by a piezoelectric transducer and transmitted into a solid buffer rod, which is needed to dissipate the heat of the high temperature fluid. Subsequently, the waves propagate through the rod and transmit into the fluid,then they are reflected back into the rod and received by the transducer. The measurement is compared with a reference measurement, to determine the reflection coefficient, wave velocities and the attenuation. In this way, the acoustic parameters, such as density and viscosity, can be computed for small amounts of fluids with high radioactivity and corrosiveness at high temperature.

In the executed experiment, copper is used as a material for the buffer rod and glycerol for the fluid, where their most important material properties are stated in table 3.1. The transmitted ultrasonic wave will be affected by the fluids viscous properties before propagating back into the rod. The received waves by the transducer are not only affected by these properties of the fluid but also by the elastic properties of the solid buffer rod. These effects are the so called spurious echoes and interfere with the desired signal. In figure 3.3 the spurious echoes are clearly visible with a ultrasonic measurement. The major peak at $t = 2.2 \times 10^{-5} s$ represents the incident wave and the other great peak at $t = 5.7 \times 10^{-5} s$, $9.3 \times 10^{-5} s$ and $1.3 \times 10^{-4} s$ represent the reflections at the end of the rod and their repetitions. All the other minor peaks are the spurious echoes. [1]

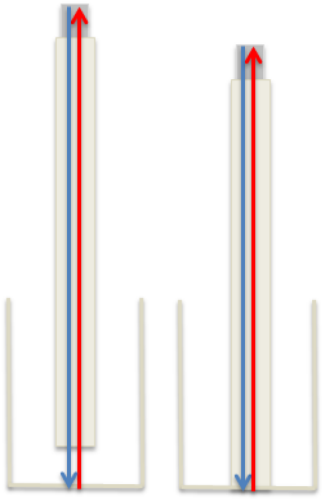

Figure 3.1: Propagation of waves through fluid and reference measurement to determine the acoustic parameters [1]

Table 3.1: Properties of used materials at room temperature (298K)

	Density [kg/m^3]	Speed of longitudinal waves [m/s]	Speed of transverse waves [m/s]	Viscosity [mPa s]
Copper	8930	4760	2325	-
Glycerol	1260	1920	-	950

3.1. Normal Incidence and Captured Waves

The transmitted waves by the transducer are plane waves. These waves are reaching the end of the rod at normal incidence, what can be seen in the figure 3.2. Therefore the reflection coefficient (2.35) and transmission coefficient (2.36) for the fluid-solid interface are simplified enormously and will be

$$R = \left(\frac{Z_L - Z_F}{Z_L + Z_F} \right)^2, \tag{3.1}$$

$$T_L = 1 - R = \frac{4 Z_F Z_L}{(Z_L + Z_F)^2}. \tag{3.2}$$

Due to this impedance difference the reflection coefficient is relatively large compared to the transmission coefficient. So the waves in the fluid are barely able to transmit into the solid and the waves are captured in the fluid. This has to be taken into account, for analyzing the experimental results.

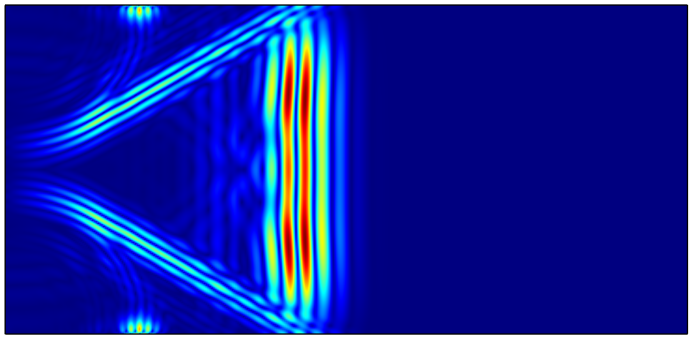

Figure 3.2: Normal incidence of the first wavefront resulting in an enormous simplification of reflection and transmission coefficients

3.2. Attenuation

Attenuation is energy loss of sound propagation due to dissipation by the viscous properties of fluids. This leads to a significant reduction of the amplitude of the waves. For the investigation of this energy consumption we are considering the one-dimensional plane wave solution

$$p = p_0 e^{\pm i(kx - \omega t)}, \tag{3.3}$$

with angular frequency ω and wavenumber k equal to $\frac{\omega}{c}$. Inserting this plane wave solution into the acoustic wave equation for viscous fluids (2.7) gives

$$(1 + i\omega \frac{4}{3} \frac{\mu}{\rho_0 c_0^2}) k^2 - \frac{\omega^2}{c_0^2} = 0, \tag{3.4}$$

that can also be written as

$$k = \pm \frac{\omega}{c} (1 + i\omega \frac{4}{3} \frac{\mu}{\rho c^2})^{-\frac{1}{2}} = \pm \beta_F - i\alpha_F, \tag{3.5}$$

and inserted back into the plane wave solution we obtain

$$p = p_0 e^{-((\beta_F - i\alpha_F)x - \omega t)} = p_0 e^{-\alpha_F x} e^{i\omega(t - \frac{x}{\omega \beta_F})}. \tag{3.6}$$

Solving equation (3.5) gives the attenuation coefficient α_F by apply Taylor expansion for $\alpha_F = \frac{1}{2} \frac{\omega}{c} \sqrt{6(9+\varepsilon)^{-1/2} - 18(9+\varepsilon)^{-1}}$, considering $\varepsilon = \frac{16\omega^2 \mu_F^2}{\rho^2 c^4} \ll 1$ [14]:

$$\alpha_F = \frac{1}{2} \frac{\omega}{c_F} \sqrt{\frac{1}{9} \frac{16\omega^2 \mu_F^2}{\rho_F^2 c_F^4}} = \frac{2\omega^2 \mu_F}{3\rho_F c_F^3}. \tag{3.7}$$

Doing the same approximation for wavenumber β_F:

$$\beta_F = \frac{\omega}{c_F}. \tag{3.8}$$

The magnitude of the attentuation coefficient α_F determines how fast the peak amplitude decays in space. Moreover, the attenuation coefficient increases quadratic with the frequency and is a function of unknown parameters viscosity and density. The attenuation coefficient can be determined by measuring the relative amplitude reduction with

$$e^{-2\alpha_F d} = \frac{A}{A_{ref}}, \tag{3.9}$$

where d is the thickness of the fluid. A and A_{ref} are the wave amplitudes. Using (3.1) and (3.2) the density can be determined by considering normal incidence of the incoming waves at the solid-fluid interface, i.e. $\cos\alpha = \cos\gamma = 1$ and $Z_1 = c_F\rho_F$.

$$\rho_F = \frac{Z_2}{c_F}\left(\frac{1-R}{1+R}\right), \tag{3.10}$$

where Z_2 is the acoustic impedance of the buffer rod. For (3.10) the reflection coefficient can be determined by measuring the amplitude difference of the signal with a reference measurement [1]

$$R = \frac{A}{A_{ref}}R_{ref}. \tag{3.11}$$

3.3. Conclusion

Since normal incidence of the waves at the interface of the rod and the fluid, equations (2.35) and (2.36) are simplified into equations (3.1) and (3.2). With the properties of copper and glycerol, 79.8% of the energy reflects and 20.2% transmits at their interface. Consequently, ultrasound waves in the fluid cannot transmit directly back into the buffer rod and are practically 'captured' in the fluid.

Using (3.10) and (3.7) the density and viscosity of a fluid can be determined by measuring the velocity and amplitude of the reflected waves.

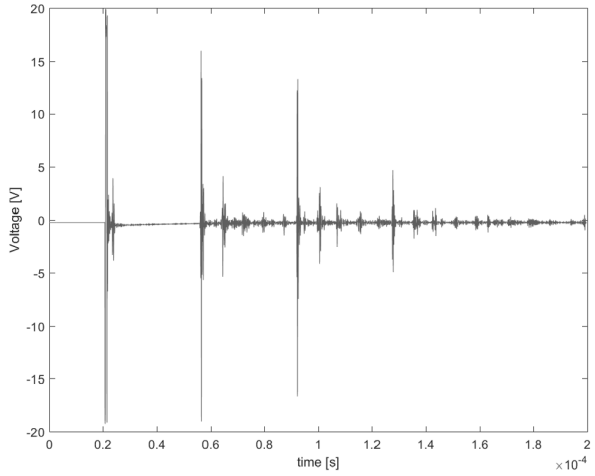

Figure 3.3: Measured signal of [1], consisting of the initial signal and its repetitions (major peaks) and the spurious echoes in between

II

Simulation of Ultrasound

4

Simulation Model

In order to investigate the causes of spurious echoes for ultrasonic measurements, a simulation model is created to visualize the behavior of the ultrasonic waves. For the simulations the software COMSOL Multiphysics is used, what has ingrained physical expressions and the material characteristics. The software is based on Finite Element Method to solve the differential equations by transform them into discrete intervals. This discretization will be discussed in a later section. With COMSOL different problems can be studied: frequency domain and time domain study, stationary study, eigenvalues study and eigenfrequency study. In this research we are interested in the time domain study, as the emitted ultrasonic waves are finite signals.

The setup of the executed experiments consist of three domains: the transducer, the solid buffer rod and the liquid fluid,of which the properties have to be determined. The simulation of the transducer will be treated in later section. The simulation of the fluid domain has not been our interest, since firstly we want to investigate the behavior of the sound waves in the buffer rod resulting in spurious echoes. In this section we are going to focus on the solid domain, i.e. the buffer rod. For this domain the module *Solid Mechanics* has been used, where the elastic vibrations described in displacement. The geometry is reduced to a simpler two-dimensional problem with Cartesian coordinates. This is done to prevent excessively long computation time, that makes unattractive working with three-dimensional models. In a subsequent research, this can still be investigated.

4.1. Boundary Conditions

There are two boundary conditions to consider: one that simulates the transducer and one that take in consideration the external surface of the rod. Since we only consider the solid rod and exclude the whole fluid domain, the rod is totally enveloped with air. As we saw in previous section at page 14 this interface could be considered as free boundary, where the surrounding air could be simulated as vacuum and only reflections occur. In COMSOL it means the boundary condition *free*. With this boundary condition it results in are no constraints and no loads acting on the boundary.

The decision which boundary condition has to function as a transducer depends on what you want to measure. Because next to generating ultrasonic waves the simulated transducer has to be able to detect and reflect the incoming reflected waves as well. Taking this into account there are two possible boundary condition suitable for simulating the transducer

- *Pressure load*
- *Prescribed displacement*

The pressure load condition has expression $\vec{\sigma} \cdot \vec{n} = -p\vec{n}$ at the boundary, which implies that the stress will be always keep zero after the function of the source. So this boundary condition is useful when measuring displacements of the solid at the place of the transducer. The prescribed displacement has function $u = u_{0x}$

at the position of the transducer and is therefore suitable for measuring pressure, but not for measuring the displacement. The transducer's amplitude will be simulated as an infinite sinus with frequency of 3.5 MHz with Gaussian window with a standard deviation of $\frac{3.5}{6}$ period of the sinus, see figure 4.1. The Gauss function is considered zero after three standard deviation steps. [7]

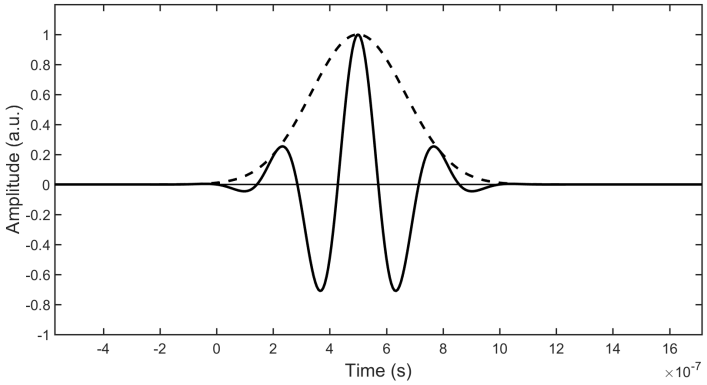

Figure 4.1: Wave packet as boudnay source consisting of sinus (f=3.5[MHz]) with Gaussian window

4.2. Discretization

Wave propagation simulation are currently done with finite element method by dividing the time-domain of the solution into small intervals, time-steps. In much the same way the spatial-domain is divided into small spatial elements by a mesh. There will be always strived to minimize the number of spatial elements and time-steps to allow the calculations to be performed in a reasonable time. However, there is an important consideration in both spatial- and time-domains. Does the amount of spatial/time elements permit the features of the solution to evolve accurately? For the simulation of waves this generally depends upon the frequency and the wavelength of the wave, which is related to the Nyquist-rate: the mesh size has to be smaller to the half the wavelength to generate no errors and likewise the time-step size has to be smaller than half the period of the highest frequency of the wave to prevent errors [21].

In our setup the frequency will keep always the same, but the longitudinal and transverse waves differ from wavelength. By the Courant–Friedrichs–Lewy (CFL) condition the time step can be determined by $t_{step} = \frac{\lambda_S}{CFLc_L}$, where literature studie say that a CFL of 0.2 is near optimal [22, 23]. In addition, the time step has to be rather the small, to be sure that the solution will be accurate, therefore c is c_L and λ is λ_S.

The quality of the mesh is of great importance to retrieve accurate results. A balance has to be found between accuracy and computation time. The mesh is a mapped mesh distributed over the edges of the geometry where the number of mesh element is determined by $\# = N\ \frac{length}{\lambda_S}$. With N is the number of mesh element per wavelength. After investigation of times of peak values of signals with different amount of mesh elements, can be concluded that eight mesh elements is the minimum amount of mesh elements per wavelength that produce accurate simulation outcomes. The delay times of the peaks values for signals with a different amount of mesh elements per wavelength are stated in figure 4.3

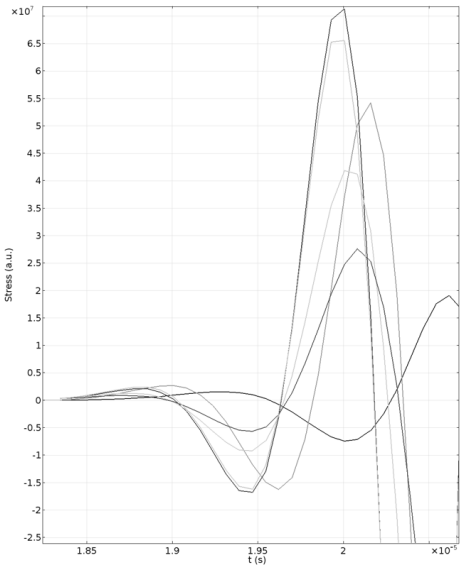

Figure 4.2: Signals with different times of peak values for determination of the influence of the total amount of mesh elments

Once a Nyquist-error emerges it will propagate throughout the solution and it can evolve to dominate the solution. In severe

cases, the calculation will be terminated by the convergence criterion in the solver. In less severe cases a solution will be found which does not represent physical behavior properly. It can be difficult to detect this error, so it is essential to have a critical attitude towards the simulation outcome. The numerical solutions has to be checked by the physical knowledge. Despite the failures, the poorly-configured model still produces results that have some physical correctness. Failures of poorly configured models [21]:

- Wave-fronts appearing ahead of the first wave-front, producing an erroneous dispersion effect
- Waves appear to reverberate inside the transducer for much longer that well-configured models predict

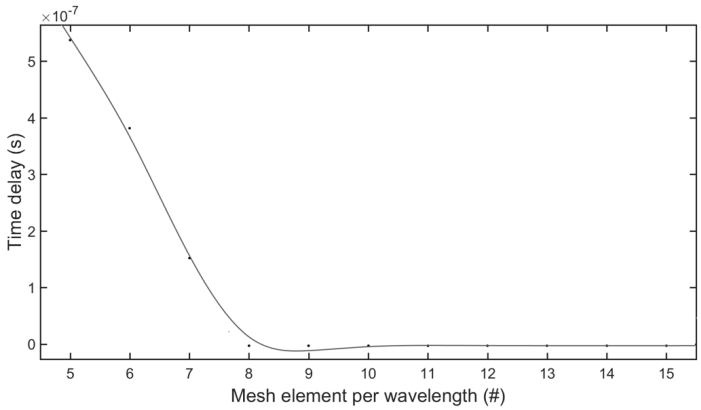

Figure 4.3: Time delay of signals for increasing number of mesh elements

4.3. Conclusion

To prevent excessively long computation time, the simulation model is performed with a two-dimensional geometry. However, the two-dimensional domain does not take into account the axial interaction and the simulation outcome will be slightly different with the reality. For more accurate simulation and being able to compare the results with the experimental measurement, a three-dimensional geometry have to be used. However, first three-dimensional simulation show a non-linear relation for different source amplitudes. In next research a amplitude source has to be determined, which matches with the behavior of the transducer.

For the simulated transducer emitting a finite signal with constant frequency a sinusoidal signal with a Gaussian window will used as source. The boundary condition driven by this source will be a displacement condition, in order to have no constraints in the stress. Therefore we are able to measure in the same quantity as pressure for fluids, in the end.

Accurate simulation outcomes require minimal eight mesh elements per wavelength. For the time-stepping is the Courant–Friedrichs–Lewy (CFL) condition applied and based on other literature studies considered with five time intervals in each period. In subsequent research, this number can be optimized as well, for more efficient calculations.

5

Simulation Results

In the previous section we treated all settings in COMSOL in order to make an accurate simulation of ultrasonic waves. In this section we are going the look at the simulation and will seek about the causes of spurious echoes. In figure 5.1 one can see an image of a propagating wave front in the buffer rod. We will focus on three probable causes of the spurious echoes: head waves, longitudinal wavefronts and ratiated edge waves.

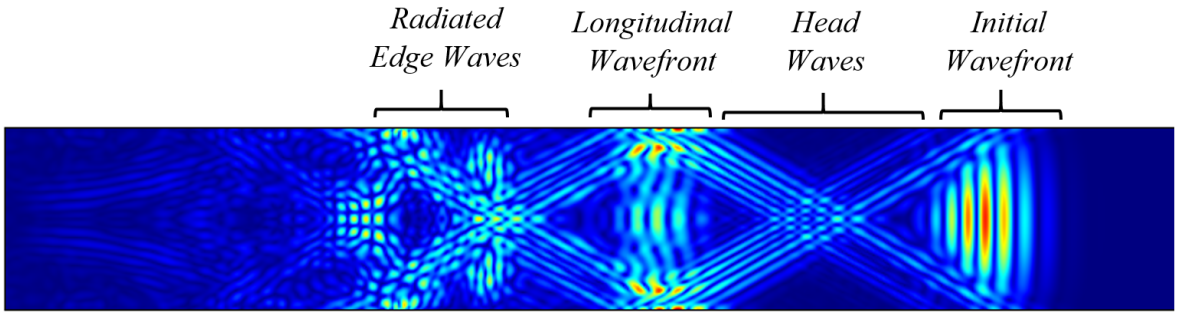

Figure 5.1: Propagation of ultrasonic waves (f=2[MHz] in a copper buffer rod at $t = 2.4 \cdot 10^{-5}[s]$. The simulation consist of four types of waves, including the spurious echoes

5.1. Mode Converted Head Waves

The initiated wavefront with longitudinal wave is propagating almost over the whole width parallel to the rod's longitudinal axis. In figure 5.2 the direction of the displacement of the local particles are given by the arrows. In this figure it can be seen that for the waves in the initial wavefront the displacement of the particles is in the same direction as the direction of the wave. Because of the rod's finite diameter, these collide with the edge of the rod, resulting in continuous reflections consisting of longitudinal and shear waves. Since the longitudinal waves propagate nearly parallelly to the longitudinal axis, the angle of incidence is almost 90°. In figure 2.8 can be seen that for a copper rod most of the reflected waves are longitudinal waves, for those incident angles. The vast minority of the reflected waves are shear waves and following Snell's law (2.23) reflected with an angle of 29.2°, for copper. The angle difference between those reflected of those waves is 60.8°. The proof that these refracted waves are shear waves can be given by measure the actual angle between the reflected waves in figure 5.2.

In figure 5.2 the particle movements of the local particles are parallel with the intensity lines, it suggest that the combination of all particles vibrations forsm shear waves. The measured angles between the perpendicular line of the those displacements and the direction of the waves in the initial wavefronts corresponds with the earlier mentioned angle of 60.8°. **Together this is a proof that these waves are shear waves, produced by the longitudinal waves in the initial wavefront.** [7, 24]

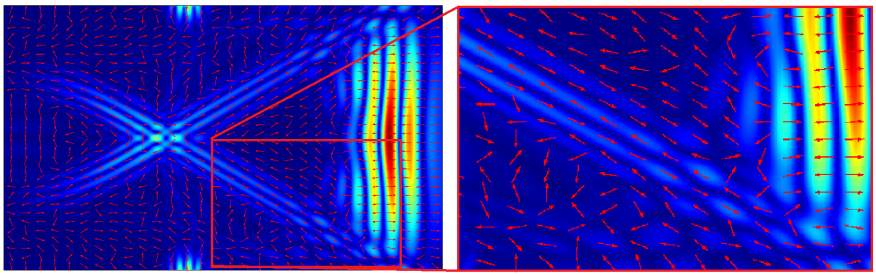

Figure 5.2: Longitudinal displacement and transverse displacement
for longitudinal and shear waves, respectively, in copper rod

These waves are called head waves instead of normal shear waves, because they seem to propagate at the speed of longitudinal waves, while they are shear waves. The explanation of this phenomenon is that the 'production' of the waves at the edge of the rod taken place at the location where the waves in the wavefront impinge this edge, that is moving with the longitudinal wave speed along the longitudinal axis.

The reflected head waves form a slanting line to the opposite edge because they are reflected with a certain angle with the longitudinal waves and they are propagation with a speed which is generally around half the speed of the longitudinal waves. The angle and the intensity of the head waves depend on the angle of the incident wave and the material properties of the buffer rod. Figure 5.3 shows a reflection reduction of 10% by changing the material for the buffer rod from copper to lead ($c_L = 2160[^m/_s], c_S = 700[^m/_s]$). **Even though, the reflection coefficient remains relatively small for incident angle of almost 90° but it will be still a important phenomenom and will be treated in next section**

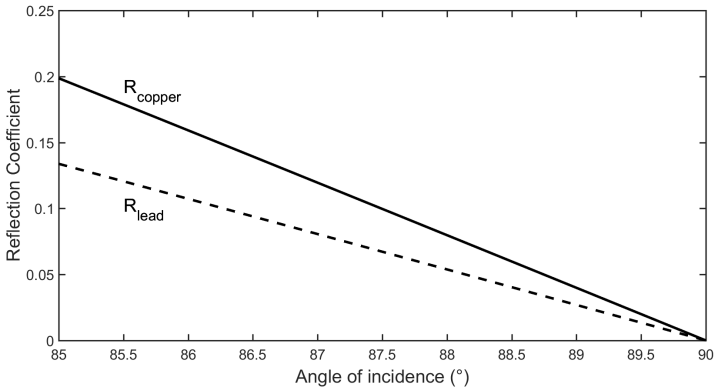

Figure 5.3: Reduction of mode conversion with lead as buffer rod material

5.2. Mode Converted Longitudinal Wavefronts

When the head waves strike to the opposite edge of the rod there will be again reflection of two waves, but this time with an incident shear wave instead of an incident longitudinal wave. Figure 2.9 shows the reflection coefficients for the longitudinal and shear waves for this incident shear waves. It appears from this figure that approximately 2/3 of all reflected waves are longitudinal waves, and is relatively much mode converted reflected waves, comparing it with the fraction of produced shear waves from the waves in the intitial wavefront. The new longitudinal waves from the head waves will travel with the same velocity as the initial wavefront and are directed almost parallel to the longitudinal axis of the rod.

The incident angle of the head waves is equal to their previous refracted angle, which is just below the critical angle. When the angle of incidence is larger than the critical angle then all the reflected waves would be shear waves and not longitudinal waves. But this is impossible, since waves of the initial wavefront cannot impinge the edge with a angle of 90° or larger.

The intensity of the produced longitudinal waves will become almost as great as the initial wavefront. Due to the continuous production of head waves, the production of the longitudinal by these head waves is large as well. Once, converted from head waves back into longitudinal waves, the longitudinal waves will propagate again with the velocity of the longitudinal waves and all new longitudinal waves gather at the same place. Therefore, the waves develop into a new wavefront with increasing intensity. **Due to this increasing intensity this phenomenon has a great contribution to the spurious echoes.**

5.3. Radiated Edge Waves

The transducer should generate solely longitudinal waves propagating purely as plane waves along the longitudinal axis. Transducers, however, have the side effect of producing edge waves as well. It is well-known these edge waves propagate as diffracted longitudinal waves through the rod. Because of their smaller angle of incidence they amplify the production of the head waves. However, the simulations show that the transducer seems to produce shear edge waves as well. These waves can be seen in figure 5.4 and can be recognized by their wave velocity, which is half the speed of longitudinal waves.[25]

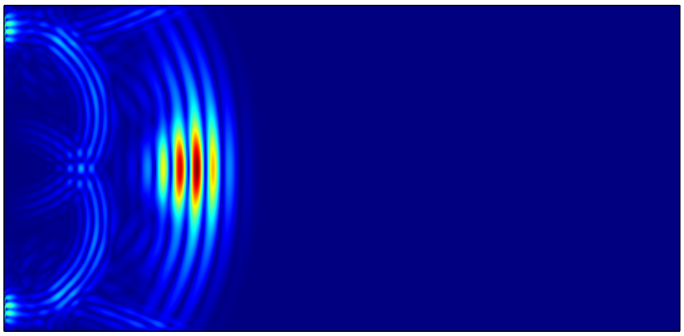

Figure 5.4: Radiation of edge waves, consisting of longitudinal and shear waves for a transducer with RR = 0.30

The intensity of shear waves depends on the maximum amplitude of the transducer and the incident angle of these waves are dependent on the ratio of the transducer and the width of the buffer rod. The width of a transducer can be defined as a RR-number, where $RR = \frac{R_{transducer}}{R_{rod}}$. Figure 5.5b shows the spurious echoes caused by a wide transducer, with RR=0.90. Due to the chancing incident angles of the radiated shear waves and therefore no structural behavior at the boundaries, **let us conclude that the radiated shear waves causing random noise and therefore will not contribute greatly to the spurious echoes.**

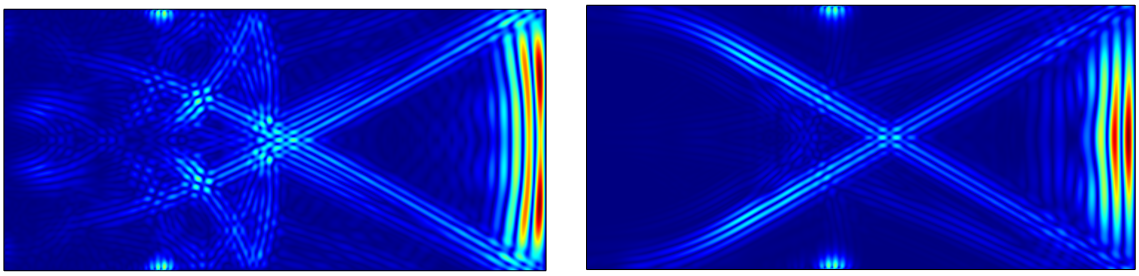

(a) Radiated shear waves for transducer of RR=0.3 (b) Absence of shear waves for transducer of RR=0.9

Figure 5.5: Relative low contribution of the limited diameter of transducer to the spurious echoes

5.4. Conclusion

Spurious echoes are clearly visible in the simulations. Based on the simulations one can divide the echoes created in the buffer rod into three types: head waves, longitudinal wavefronts and edge waves. Regarding to the intensities the head waves and the edge waves are considered as non-significant for the contribution of the spurious echoes. Though, the head waves create additional longitudinal wavefronts when impinge on the opposite edge. These longitudinal waves have a high contribution to the spurious echoes. Therefore the head waves are important for the reduction of these spurious echoes.

Next, the simulations show that the transducer seems to produce shear edge waves as well. In subsequent research the presence and possible contribution of these shear edge waves has to be investigated.

6

Conclusion and Recommendation

For the investigation of the ultrasonic waves in the buffer rod a simulation model is made. In this research is shown that accurate simulations require minimal eight mesh elements per wavelength. Less mesh elements lead to false simulations, where more element result in unnecessary long computation time. The time step is assumed from literature studies, with the CFL-number set to 0.2. An optimal CFL-number has to be investigated in subsequent research, for more efficient calculations. To prevent excessively long computation time, the simulation model is performed with a two-dimensional geometry. However, the two-dimensional domain does not take into account the axial interaction and the simulation outcome will be therefore slightly different from reality. For more accurate simulation and being able to compare the results with the experimental measurement, a three-dimensional geometry has to be used. However, three-dimensional simulation show a non-linear relation of the amplitude and the simulation outcome. This influence of the amplitude has to be investigated in a next research.

In the experimental measurements, the spurious echoes are present between the peaks of the initial wave's reflection and its repetitions. Spurious echoes are caused by multiple phenomena. First, impedance difference of the fluid and the solid rod lead to 'captured' waves, since the waves in the fluid are barely able to transmit into the solid and the waves are captured in the fluid.

Next, complex interaction of waves in the buffer rod causes new waves, which interfere with the captured waves. These waves are clearly visible in the simulation and can be divided into three types of waves. The waves with the largest contribution to the echoes are the new longitudinal wavefronts. Once reflected as longitudinal waves, the waves will propagate with the velocity of the longitudinal waves and all new longitudinal waves gather at the same place. Therefore, the waves develop into a new wavefront with increasing intensity with a large contribution to the spurious waves. Secondly, since the rod has a finite diameter, initially emitted waves collide with the edge of the rod, resulting in continuous reflections. The reflected waves consisting of longitudinal and shear waves. The shear waves are called head waves and seem to propagate at the speed of longitudinal waves, while they are shear waves. These waves are interesting, because they create the longitudinal wavefronts, when impinge on the opposite edges. We have seen in the theory that the production of those head waves at a free boundary are dependent on two parameters: speed of sound waves and the incident angels. Optimization of these parameters can cease the production of the head waves, resulting in reduction of the spurious echoes. In this research we have shown that the production of head waves can be reduced with 10%, by replacing the copper rod for a lead rod. Tapering or cladding of the buffer rod suggested from other studies seem to be good alternatives to reduce the spurious echoes.

Next, the simulations show that the transducer seems to produce shear edge waves as well, what is extraordinary for a longitudinal transducer. In subsequent research the presence and contribution of these shear edge waves have to be investigated.

In this research, the waves are manually distinguished based on the direction of particle motion. Since all waves have different velocities, it could be helpful in a next research, to measure the waves by its wavenumber. Because, for the reduction of the spurious echoes a quantitative measuring method is essential.

A

Reynolds Transport Theorem

Both acoustic and elastic waves equation are based on the fundamental laws of continuum mechanics describing the conservation of mass, momentum and energy. All these conservation laws are based on the Reynolds transport theorem [11] and can be expressed for a vector or scalar-valued function $\vec{f}$ in a domain

$$\frac{d}{dt}\int_{\Omega} f\,dV = \int_{\Omega}\frac{\partial f}{\partial t}\,dV + \int_{\partial\Omega}(\vec{v}\cdot\vec{n})f\,dS, \tag{A.1}$$

where $\partial\Omega$ is the boundary of the domain Ω with volume V and surface S. $\vec{n}$ is the outward unit normal vector to the boundary and $\vec{v}$ is the velocity field. The first integral is the time rate of change of f following the motion. The second integral is the rate of change of f stored in the domain and the last integral is the net outflux of f across the surface. We concentrate on the conservation of mass, momentum and energy in order to derive the acoustic wave equation, where a pressure increase is applied at the plate of the origin, hence particles will flow to the right, leading to an alternative compression and rarefactions. The conservation of mass in a fluid flow requires that the change of mass inside a control volume is accounted for the net flow of mass across the surface since mass cannot be created or destroyed within the control volume. Reynold's transport theorem obeys this by for the substitution of ρ for function f and gives the integral

$$\frac{\partial}{\partial t}\int_{\Omega}\rho\,dV + \oint_{\partial\Omega}\rho\vec{v}\,dS = 0. \tag{A.2}$$

This relation is called the equation of continuity and describes that the rate of change of mass inside the control volume plus the net rate of outflow of mass across the control volume surface add to zero. The momentum of the fluid in a material volume is the integral of the momentum per unit volume $\rho\vec{v}$ over the material volume. The integral form of the time rate of increase of momentum within the control volume is given by substituting $\rho\vec{v}$ into the Reynold's transport theorem expression

$$\frac{d}{dt}\int_{\Omega}\rho\vec{v}\,dV = \int_{\Omega}\frac{\partial\rho\vec{v}}{\partial t}\,dV + \int_{\partial\Omega}((\rho\vec{v})\cdot\vec{n})\vec{v}\,dS). \tag{A.3}$$

To apply Newton's law of motion to the material volume that coincide with our control volume at a particular time, we have to determine the forces that act on the fluid within the control volume. Neglecting the viscous effects and the gravitational forces, the only force that is acting on the fluid will be the force caused by pressure p acting inward on the control surface S. Combining this pressure force with the Reynold's transport theorem will give

$$\frac{d}{dt}\int_{\Omega}\rho\vec{v}\,dV=\int_{\Omega}\frac{\partial\rho\vec{v}}{\partial t}\,dV-\oint_{\partial\Omega}(-p\vec{v})dS. \tag{A.4}$$

Supposing that the variations of the pressure are small compared with the steady-state pressure, so the middle term can be neglected. Lastly, the conservation of energy can be fullfilled if we substitute $f=\rho(u_{int}+\frac{\vec{v}^2}{2}+\vec{g}z)$, with u_{int} as the internal energy and g as the gravitational constant. But in the report we have made some simplifications for solving the conservation of energy. The conservation laws may be written in integral or differential form. The integral formulations are used to describe the change of mass, momentum or energy within the volume, where the differential formulation yields an expression which may be interpreted as the integral form applied to an infinitesimally small volume. We can consider Ω as an infinitesimal volume to obtain the differential equation of the conservation laws. The flux of a vector field through a surface can be related to the behavior of the vector field inside the surface by Gauss's theorem, called the divergence theorem

$$\oint_{\partial\Omega}(\vec{f}\cdot\vec{n})\,dS=\int_{\Omega}(\vec{\nabla}\cdot\vec{f})\,dV. \tag{A.5}$$

Bibliography

[1] S. Mastromarino, *Determination of Thermodynamic properties of Molten Salt*, Ph.D. thesis, University of Technology Delft (2016).

[2] G. Locatelli, M. Mancini, and N. Todeschini, *Generation iv nuclear reactors: Current status and future prospects,* Energy Policy **61**, 1503 (2013).

[3] Unknown, *Overview: the thorium molten salt reactor,* ().

[4] C.-K. Jen, B. Cao, K. Nguyen, C. Loong, and J.-G. Legoux, *On-line ultrasonic monitoring of a die-casting process using buffer rods,* Ultrasonics **35**, 335 (1997).

[5] T. Ihara, N. Tsuzuki, and H. Kikura, *Development of the ultrasonic buffer rod for the molten glass measurement,* Progress in Nuclear Energy **82**, 176 (2015).

[6] I. Ihara, *Ultrasonic sensing: fundamentals and its applications to non-destructive evaluation (a draft),* Nagaoka University of Technology. Jepang (2008).

[7] W. Ke and S. Chaki, *Finite element simulation of the critically refracted longitudinal wave in a solid medium,* in *10ème Congrès Français d'Acoustique* (2010).

[8] Unknown, *Acoustic-Structure Interaction Creates Sound*, COMSOL Multiphysics Cyclopedia ().

[9] N. Earth Observatory of Singapore, *Why s-waves cannot travel through liquids?* .

[10] Unknown, *Fluid Mechanics and Properties of Fluids*, University of Leeds ().

[11] S. Mönkölä, *Numerical simulation of fluid-structure interaction between acoustic and elastic waves,* Jyväskylä studies in computing; 1456-5390; 133. (2011).

[12] J. D. N. Cheeke, *Fundamentals and applications of ultrasonic waves* (CRC Press LLC, 2002).

[13] J. van Hoof, *One- and two-dimensional wave propagation in solids*, Master's thesis (1994).

[14] S. Mastromarino, *Wave propagation in viscous fluid*, Ph.D. thesis, University of Technology Delft (2016).

[15] K. W. van Dongen and F. Bociort, *Course advanced wave propagation*, University of Technology Delft.

[16] Unknown, *Reflection and transmission coefficients*, Stanford Exploration Project ().

[17] N. T. N. R. Center, *Mode conversion,* .

[18] P. Hora and O. Cervená, *Fem simulation of an integrated longitudinal and tangential wave probe,* .

[19] U. Paris-Saclay, *Reflection and refraction of ultrasonic waves,* .

[20] A. Bouhadjera and F. Schubert, *An ultrasonic mode conversion technique for characterising prismshaped samples–experimental and numerical results,* in *9th European conference on NDT, Berlin, Germany* (2006).

[21] D. Andrews, *Modelling of ultrasonic transducers and ultrasonic wave using finite elements,* 2014 COMSOL Conference Cambridge .

[22] Hisham, *Comsol convergence tips,* .

[23] B. Ghose, K. Balasubramaniam, C. Krishnamurthy, and A. S. Rao, *Two dimensional fem simulation of ultrasonic wave propagation in isotropic solid media using comsol,* in *COMSOL Conference* (2010).

[24] W. Hassan and W. Veronesi, *Finite element analysis of rayleigh wave interaction with finite-size, surface-breaking cracks,* Ultrasonics **41**, 41 (2003).

[25] J. P. A. T. J. C. M. G. J. S. J. Garcia-Alvarez, Y. Yanez, *Noise level analysis in buffer rod geometries for ultrasonic sensors,* (2006).